Simulating the *Weak* Death of the Neutron in a Femtoscale Universe with Near-Exascale Computing

Evan Berkowitz[*], M.A. Clark[†], Arjun Gambhir[‡§¶], Ken McElvain[¶§], Amy Nicholson[‖], Enrico Rinaldi[**§], Pavlos Vranas [‡§] André Walker-Loud [§‡¶], and Chia Cheng Chang[§¶††], Bálint Joó[‡‡], Thorsten Kurth[x§], Kostas Orginos[xi xii],

[*] Institut für Kernphysik and Institute for Advanced Simulation, Forschungszentrum Jülich, 54245 Jülich Germany
[†] NVIDIA Corporation, Santa Clara, California, 95051, USA
[‡] Physical Sciences Directorate, Lawrence Livermore National Laboratory, Livermore, California 94550, USA
[§] Nuclear Science Division, Lawrence Berkeley National Laboratory, Berkeley, CA 94720, USA
[¶] Department of Physics, University of California, Berkeley, CA 94720, USA
[‖] Department of Physics and Astronomy, University of North Carolina, Chapel Hill, NC 27516-3255, USA
[**] RIKEN-BNL Research Center, Brookhaven National Laboratory, Upton, NY 11973, USA
[††] Interdisciplinary Theoretical and Mathematical Sciences Program, RIKEN, 2-1 Hirosawa, Wako, Saitama 351-0198, Japan
[‡‡] Scientific Computing Group, Thomas Jefferson National Accelerator Facility, Newport News, VA 23606, USA
[x] NERSC, Lawrence Berkeley National Laboratory, Berkeley, CA 94720, USA
[xi] Department of Physics, The College of William & Mary, Williamsburg, VA 23187, USA
[xii] Theory Center, Thomas Jefferson National Accelerator Facility, Newport News, VA 23606, USA

***Abstract*—The fundamental particle theory called Quantum Chromodynamics (QCD) dictates everything about protons and neutrons, from their intrinsic properties to interactions that bind them into atomic nuclei. Quantities that cannot be fully resolved through experiment, such as the neutron lifetime (whose precise value is important for the existence of light-atomic elements that make the sun shine and life possible), may be understood through numerical solutions to QCD. We directly solve QCD using Lattice Gauge Theory and calculate nuclear observables such as neutron lifetime. We have developed an improved algorithm that expoentially decreases the time-to-solution and applied it on the new CORAL supercomputers, Sierra and Summit. We use run-time autotuning to distribute GPU resources, achieving 20% performance at low node count. We also developed optimal application mapping through a job manager, which allows CPU and GPU jobs to be interleaved, yielding 15% of peak performance when deployed across large fractions of CORAL.**

I. Justification for ACM Gordon Bell Prize

Our algorithm *exponentially decreases time to solution* by accessing parameter space where the signal-to-noise is exponentially larger. Our code is optimally mapped on the machine and our kernel can "auto-tune" local GPU resources at runtime. We achieve excellent scaling across large fractions of the CORAL supercomputers achieving a peak sustained performance in excess of 15%.

II. Performance Attributes

Attribute	Value
Category of achievement	time to solution
method	explicit
reporting	whole application including I/O
precision	mixed-precision
system scale	full-scale system
measurement method	FLOP count

TABLE I
PERFORMANCE ATTRIBUTES

III. Overview

The Standard Model (SM) of particle physics is the currently accepted (and incredibly well-tested) theory describing fundamental particles and their interactions, which give rise to all ordinary matter in the universe. Calculations of properties of matter directly from the SM can give us unique insight into some of the outstanding questions about our universe that are difficult or impossible to address with experiment. For example, when compared to all other atomic nuclei, the simplest bound nucleus, Deuterium (one proton and one neutron), has an anomalously small binding energy per constituent. This small energy has huge consequences for the evolution of life as we know it, in part from its contribution to the very slow fusion process which has heated our Sun for the last 4.6 billion years and prevents it from collapsing under its own gravity. The question, then, is whether this anomalous value is a chance consequence of fine-tuning of the parameters of the SM, or a more robust, fundamental property of the theory; only direct calculations from the SM may provide an answer.

The lifetime of the neutron is an equally important quantity for the evolution of the universe as we know it. Free neutrons end their lives by decaying into a proton, electron, and anti-neutrino within an average time of about 14 minutes. In contrast, when bound in nuclei, such as Deuterium, or Helium (He) (2 protons and 1 or 2 neutrons), neutrons become stable, and their lifetime, infinite. This stability has importance consequences: in the first few minutes after the Big Bang, as the universe was expanding and cooling, free neutrons

SC18, November 11-16, 2018, Dallas, Texas, USA
978-1-5386-8384-2/18/$31.00 ©2018 IEEE

decayed, with the resulting protons later binding with electrons to form Hydrogen atoms. Some neutrons were saved from this decay by being bound into light nuclei, such that the primordial universe was composed of approximately 75% Hydrogen (H) and 25% ^{4}He by mass fraction, or rather, there was approximately 1 neutron for every 7 protons. Had the neutron lifetime differed from this value, H and He would have formed at different rates and the universe today would be quite different. For example, this initial abundance of hydrogen is critical to the formation of stars, including our Sun.

The neutron lifetime can be precisely measured experimentally. However, current results coming from two different measurement techniques (trapped neutrons versus neutron beams) disagree significantly: $\tau_n^{trap} = 879.4(6)s$ and $\tau_n^{beam} = 888(2)s$ [1], [2]. This has raised the exciting possibility that there may be new, unknown physics contributing to the neutron decays which gives rise to this difference [3], [4], [5].

To decide whether new physics causes this discrepancy, we must first confidently know the neutron lifetime as predicted by all known physics and then compare it to experimental results. The SM of particle physics makes a definite prediction (recently updated in Ref. [2]), a lifetime of

$$\tau_n = \frac{5172.0 \pm 1.0}{1 + 3g_A^2} \text{ seconds.} \tag{1}$$

The *axial coupling of the neutron*, g_A, dictates the strength of the *weak* interaction with protons and neutrons, and has implications beyond the neutron lifetime. For example, it is also a key quantity in determining the rate of solar fusion as it dictates the rate of conversion of the protons in H to neutrons at high temperatures during the formation of deuterium.

The axial coupling is not an input parameter of the SM but an emergent property of neutrons, themselves made of *quarks* and *gluons* which are described by a part of the Standard Model known as Quantum Chromodynamics (QCD). Computing g_A from QCD requires high performance computing, as it entails solving the equations non-perturbatively. QCD is so *strongly interacting* that we never see isolated quarks or gluons—we only see them bound into protons, neutrons, and other *hadrons*. QCD fixes the nuclear interactions between protons and neutrons, which are strong enough to bind them into nuclei, overcoming the protons' electromagnetic repulsion.

That these interactions are so strong means that we cannot rely on pen-and-paper estimates from QCD but must resort to numerical methods instead. *Lattice QCD* (LQCD) is the formulation of QCD on a finite space-time grid, or lattice, representing a portion of our universe, which captures the correct quantum-mechanical behavior via a Monte Carlo approach. While the theory and methods are known, leveraging this approach for nuclear physics proves to be extremely demanding computationally. For example, the LQCD community previously estimated that a determination of g_A with a 2% precision would be possible by approximately 2020 with the CORAL generation of supercomputers [6]. In order to have an impact on the experimental discrepancy in the measurement of the neutron lifetime, we require a determination of g_A with a precision of 0.2% or better.

While pursuing the challenging calculation of g_A, we have developed a new physics algorithm [7] which allowed for exponential improvement over previous state-of-the-art results. We have developed new software to exploit this idea and performed a full-scale calculation of g_A using recent generations of NVIDIA-GPU accelerated compute nodes, with newly developed job management software to achieve a determination of g_A with an unprecedented 1% precision [8], [9].

This benchmark calculation showed for the first time that lattice QCD may be reliably applied to nuclear physics applications with fully controlled uncertainties, opening the door to applications to light nuclei. Even in this preliminary stage, the work was important enough to merit publication in Nature [10]. Furthermore, we have critically identified how increased calculation time can systematically and simultaneously improve the three dominant sources of uncertainty in the calculation of g_A.

In order to complete the calculation of the neutron lifetime to the precision necessary for distinguishing new physics, as well as broaden the successful application of lattice QCD to light nuclei, we must apply our techniques to multi-nucleon systems, which requires us to calculate on larger lattices, increasing their size to unprecedented proportions. With these large lattices in hand, direct calculation of nuclear properties are unlocked. Coupled with other theoretical tools, first-principles determinations may reach as deep into the periodic table as oxygen.

IV. Current State of the Art

Background

Solving the equations of QCD using numerical LQCD methods rely on fast linear solves of a very large sparse matrix whose size is determined by the size of the four-dimensional lattice used to discretize the equations (and including a fifth dimension in state-of-the-art computations). On a lattice of spatial size L and temporal size T (with extra dimension L_5) the matrix, called the Dirac operator, acts on a space of size $L^3 \times T \times L_5 \times N_c \times N_s$, where $N_c = 3$ is the size of the fundamental representation of $SU(3)$ (which describes the quark-gluon interactions), and $N_s = 4$ counts the quark spin degrees of freedom. Typical lattices are $48^3 \times 64 \times 20$ and $64^3 \times 96 \times 12$, but understanding the properties of light nuclei will require bigger ones (for example a $96^3 \times 144 \times 20$ lattice, whose Dirac operator has $\sim 10^{19}$ entries). The discretized Dirac operator is radius-one stencil kernel, and contains (complex-valued) "submatrices" along the diagonal that are small, 12×12, but dense. As is typical with stencil computations, the usual prescription is to

1) Pack the halo into contiguous buffers
2) Communicate halos to neighbors
3) Compute the interior stencil application
4) Once halos have been communicated complete halo stencil computation

In an ideal world the communication (2) can be completely overlapped with the interior GPU computation (3), and when this is achieved the computation will successfully strong scale.

Much of the computational cost for LQCD goes into using iterative Krylov-solver methods to solve the Dirac operator and obtain the so-called "propagator". For the discretization used in the present work, the so-called Möbius Domain-Wall discretization, the state-of-the art technique is to utilize conjugate gradient on the normal equations. This is the first challenge and it can be overcome by using GPU-accelerated nodes on the CORAL systems and by scaling to a larger number of nodes when the lattice size increases. By increasing the number of calculated propagators we can reduce the statistical uncertainty of the final observable, because each new propagator amounts to a new sample in the ensemble describing how quarks propagate in the lattice universe. However, the statistical uncertainty is only reduced $\propto N_{sample}^{-1/2}$.

Performance related For comparison of our code performance with the previous state of the art we use metrics that we have measured on the previous generation supercomputer, Titan. The results are shown in figure 3.

We utilize the Chroma [11] application in our work: Chroma is part of the SciDAC-funded USQCD software suite [12] that achieves portability through utilizing optimized libraries for the time-consuming portions of the QCD, e.g., the Dirac linear system solves. In the case of NVIDIA GPUs, QUDA is used [13] to allow Chroma to offload onto the GPUs. QUDA is a framework for constructing highly-optimized QCD algorithms, written using CUDA C++, with specific focus on linear-solver algorithms. High performance is achieved using techniques such as kernel fusion to minimize memory traffic, matrix-free stencil kernels, and kernel autotuning to maximize performance. Performance is maximized using mixed-precision iterative solvers, with the optimum approach for the stencil at hand being to use a red-black preconditioned *double-half* CG solver, where most of the work is done using 16-bit precision fixed-point storage (utilizing single-precision computation) with occasional reliable updates to full double precision [13].

GPU Kernel Autotuning

GPU kernel autotuning is important in order to maximize cache hit rate as well as ensure performance portability across GPU generation. The QUDA autotuner is a C++ run-time autotuner, where a brute-force search through launch parameter space is performed the first time an un-tuned kernel or algorithm is encountered. Once the optimum launch configuration is known, this is stored in a `std::map`, and is subsequently looked up on demand if and when this kernel is encountered again. Each entry in the map is given a unique identifier which stores the optimum launch parameters, as well as other metadata, such as performance metrics for the given kernel. The class structure makes it easy to manage the backup/restore of input data in the case of data-destructive algorithms, and to specify unique look-up keys for the same kernel but with slightly different parameters to ensure that a given computation is always launched with the optimum parameters.

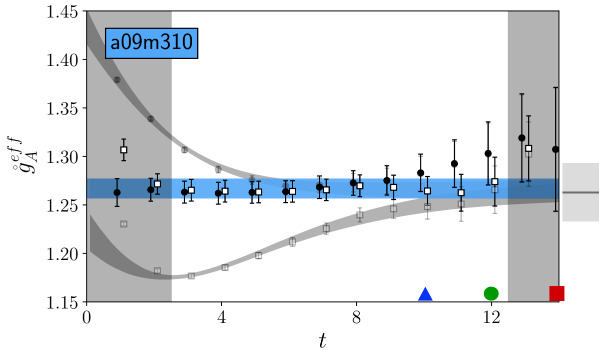

Fig. 1. Our modified results are shown in grey together with a fit to extract g_A in the large t region. The results after removing the contribution from excited neutron modelled by the fit are shown in black and white symbols. The signal is extracted from points at small temporal distances. On the contrary, traditional calculations rely on time separations indicated by the colored symbols (triangle, circle and square) at large t where the noise is exponentially larger. The blue band is our final answer, while the grey band on the right of the plot is the one obtained from a traditional calculation, which was obtained with an order of magnitude larger statistical sample.

Physics algorithms related

Traditional methods use a collection of propagators tied together to extract the neutron axial coupling g_A, by looking at its behavior for large temporal distances on the lattice. Unfortunately, the signal-to-noise ratio decreases exponentially at those large separations and shorter separations are typically not used because the signal there is affected by excited neutron effects which can systematically shift the value of g_A. It seems hopeless to try and beat an exponential decrease in statistical signal with a power law increase in samples. Therefore, the second challenge is to find new techniques yielding a final answer with an uncertainty significantly smaller by exploiting shorter temporal separations, currently missed by state-of-the-art calculations. For that reason we designed a new type of propagator [7] which yields all the temporal distances for the cost of one temporal distance in the traditional method. Using this early-time data we can determine and subtract away the systematic contamination and extract meaningful physics from very precise but otherwise uninformative data. An example of g_A obtained from our new algorithm is shown in Fig. 1. To compare with traditional LQCD calculation we notice that we can obtain a remarkably more precise answer with an order of magnitude smaller number of statistical samples [9].

V. Innovations

Dense-node Optimization

As can be seen in Table II, the transition from Titan to Sierra/Summit is more than a simple increase in speeds and feeds: the node density has also increased dramatically, with the result that there are proportionally less CPU resources to manage the GPUs. In order to minimize the CPU overhead when running multi-GPU stencil code, for communication within the node we utilize the CUDA IPC interface which faciliates direct communication between GPUs within the node. Doing so has significant benefits: the NVLink connections between GPUs in the node can be used optimally without being routed though CPU memory maximizing the exchange bandwidth between GPUs in the node. Doing so also maximizes the inter-node performance since it removes any contention for the inter-node traffic to the NIC through the CPUs. Finally, by utilizing direct CUDA DMA copies without MPI synchronization, we avoid the need to synchronize the GPU and CPU for managing the intra-node GPU transfers. This minimizes the CPU overhead: this is critical on dense-node systems where CPU resources are more contended. We note that while GPU-aware MPI does faciliate the direct transfer between GPUs in a node, we are still forced to synchronize the CPU and GPU.

The final step in this optimization is to utilize GPU Direct RDMA for inter-node transfers, i.e., direct transfers between GPUs and NIC for optimal routing of inter-node communication, further reducing CPU overheads and maximizing inter-node scaling. However, at the time of submission the Sierra and Summit systems did not support this, limiting our multi-node capability and scaling.

Communication Autotuning

In this work, we relied heavily on improvements made in the QUDA autotuner to improve the multi-node scalability, specifically extending it to include the concept of *communication-policy* tuning to pick the optimum communication approach for a given problem, at a given node count on a given target machine. While our use of backfilling and `mpi_jm` allows us to exploit the loop parallelism of the problem (see below) it is still vital to maximize the performance from exploiting the inherent data parallelism of each linear solve since we will in general need a minimum number of GPUs for a given calculation due to memory overheads, and moreover, the outer loop over which we can parallelize, while large, is finite.

When deploying multi-process stencil computations on an MPI+GPU system, there are a variety of options in how to coordinate the GPU computation with the MPI communication.

- Utilize GPU DMA engines for transferring halo buffers to and from CPU and using regular MPI on the CPU
- Utilize zero-copy reads (writes) to (from) CPU memory for MPI sends (receives) on the CPU
- Utilize GPU Direct RDMA for direct transfers between the GPU and NIC
- Whether to wait for all communication to finish and launch a single halo update kernel for all dimensions (less latency) or use fine-grained communication that can achieve better overlap

The optimal approach will depend on many factors, including:

- Whether the NIC and GPU are on the same PCIe bus
- DMA efficiency of the PCIe switch between the NIC and GPU
- GPU architecture generation (pre-Pascal GPUs were only able to saturate EDR NIC bandwidth for NIC$\rightarrow$GPU transactions but not GPU$\rightarrow$NIC)
- Message size (smaller messages are clearly more latency bound, while DMA performance may diminish at large message size)
- MPI and system software support for GPUs
- Node density, e.g., how many GPUs are sharing the same NIC

Given this multi-dimensional parameter space, and given that it is very machine specific, applying the autotuner to the stencil-communication policy is very natural. The end result is that we achieve not only performance portability across GPU generations, but also enables us to always use the optimum communication strategy regardless of the machine topology and node count we are deployed on.

Management and Backfilling of Tasks

Because of its statistical nature, a full Lattice QCD computation requires many intermediate-sized computational tasks that require different resources for different times. Naively grouping even similar tasks into a single job creates the possibility of waste, as nodes can differ in performance, and it is often advantageous to group heterogeneous tasks together. We found that naively bundling tasks—simply collecting and simultaneously launching HPC steps, and waiting for their completion—often caused a 20 to 25% idling inefficiency.

A simple solution is to *backfill* our computation, as a batch scheduler like SLURM or MOAB does. This allows us to take advantage of the otherwise wasted idle time while still occupying easier-to-schedule large allocations. As a simple proof of concept we wrote `METAQ` [14], [15], a set of shell scripts that forms a middle layer between the batch scheduler and the user's computational job scripts. This simple software allowed us to recover an enormous fraction of our wasted time, effectively providing an across-the-board 25% speed-up.

Due to its simplicity, `METAQ` is relatively hardware-agnostic and cannot, for example, guarantee that the nodes assigned to any task are near one another. Furthermore, use of `METAQ` to manage many jobs requires a separate invocation of `mpirun` (or equivalent) for each task which can become taxing on the service nodes.

As we move towards the exascale era, where many applications in addition to lattice QCD, will require the computation of thousands, hundreds-of-thousands or millions of separate tasks with different resource requirements on heterogeneous architectures, it is critical to develop user-friendly, lightweight and efficient job-management tools that will enable the full utilization of these valuable machines.

To this end, we have developed `mpi_jm`, a small library that, with just a few lines of added code, can be linked to in any application, and allows the executable to be launched with tight binding to the hardware. Closeness to the hardware combined with a high-level python interface for resource management makes for a potent and intelligent backfilling tool.

Executables linked to `mpi_jm` can be launched independently or under the management of the `mpi_jm` scheduler. That the same binary can function in both ways makes software maintenance and debugging easy.

The job manager `mpi_jm` is started as a collection of mpirun launches of a single-node manager process per node on groups of nodes (for example 32 or 128 nodes) that we call lumps. The first lump also starts a scheduler process and the remaining lumps connect to the scheduler after they initialize. The connection process uses the DPM (Dynamic Process Management) features of MPI 3.1. At the moment the only suitable MPI implementations that support the required DPM features are MPICH [16] and MVAPICH2 [17], which is built on an MPICH base.

Interconnect performance is controlled by further subdividing lumps into blocks. Blocks are configured to have a number of nodes that is a multiple of the largest jobs being run, say 4 or 8 nodes while a lump might be 64 or 128 nodes. The member nodes of a block are chosen to be close together for high performance communications. In `METAQ` we see that as jobs of different sizes complete and start again that the available nodes became fragmented, impacting performance. In `mpi_jm` the block boundaries prevent fragmentation and keep high bandwidth communications local.

The workload of jobs is defined via a python interface to an underlying C++ based scheduler. The scheduler also reads a python based description of the nodes, detailing the memory, cores, slots, and GPUs. This information is used to automatically assign ranks to appropriate nodes and slots on those nodes to efficiently access the GPUs. The scheduler has a detailed map of resources consumed by running jobs and finds good matches between ready jobs and open resources. Next a job start message is sent to a block with the open resources and it in turn uses `MPI_Comm_spawn_multiple` to start the job on the assigned resources. We made an attempt to implement a firewall against the failure of the individual job by disconnecting the intracommunicator resulting from the spawn but found that a call to `MPI_Abort` in a disconnected job still brings the entire lump down (in violation of the MPI standard), but fortunately not the entire system. This led us to use relatively small lump sizes on new systems that may be suffering from pre-acceptance issues.

Each launch of a lump is on a bounded number of nodes and hence does not suffer from the common non-linear startup cost for large sets of nodes. Any lumps that fail to start due to a node with damaged connectivity or file system problems don't connect and are ignored. Even on thousands of nodes this partitioned startup process is very fast, taking only a couple of minutes. Once the lumps have started and connected, the scheduler begins distributing jobs to the lumps where they are started in parallel. On Sierra, we were able to bring a 4224 node job up and running in 3-5 minutes, taking advantage of the lumps and MVAPICH2. In less than one minute, all lumps were connected and within five minutes, nearly all nodes were performing real work.

A major advantage of `mpi_jm` is that users can easily and safely run multiple executables on the same node. On new machines with dense nodes, when the intensive numerical work is offloaded to the GPUs, in many applications the CPUs sit idle or have very little work. With this scheduler, users can easily cut nodes into smaller pieces, or overlay GPU-capable and CPU-only tasks on the same nodes, minimizing idle cycles. This creates the possibility of taking advantage of an often-neglected additional resource, so that CPU-only tasks become effectively free.

We installed `mpi_jm` in the communications layer of the community Lattice QCD software, `QMP`[18], so that all LQCD applications can take leverage this management easily. We have used it to produce results on Sierra, ensuring we can do jobs as small as one computational task and scaling up to > 3000 nodes. On Sierra, with a large scale job, we have successfully overlapped numerically-intensive tasks that require GPUs with simpler CPU-only tasks, paving the way to hide a nontrivial computational cost.

VI. Performance Measurement Method

Overview

Because LQCD is a Monte Carlo method, for each lattice size we have a large ensemble of *gluonic field configurations* which dictate how the quarks move. The workflow is shown schematically in in Figure 2. On each configuration we solve the Dirac equation for large number of numerically expensive quark propagators. These propagators are ingredients in tensor contractions that yields the numerical data of interest; a single tensor contraction depends on more than one propagator. To control our systematic effects, such as from spacetime discretization, we use many ensembles, varying the lattice sizes and other parameters. Each ensemble requires solves for propagators and tensor contractions. For each ensemble, the propagator solves consume about 97% of the execution time, while tensor contraction consumes about 3%.

Linear Solver Performance

When reporting the linear solver performance, we utilize three performance metrics: sustained floating-point operating per second, sustained effective memory bandwidth, and sustained percent of floating-point peak. While the flops rate is a relevant measure for machine comparisons, as a relative measure of machine efficiency, sustained bandwidth is the most relevant since the limiting performance of a stencil computation should in almost all cases be bandwidth.

For reporting flops, we simply add up the necessary number of operations required in the stencil application and the auxiliary BLAS-1 operations required in the CG linear solver. This is straightforward to do, since the stencil is uniform and acts on a regular grid. For the red-black-preconditioned Domain-wall stencil used in this work, there are between 10,000-12,000 floating point operations per five-dimensional lattice point (using conventions consistent in the LQCD domain). In comparison, the BLAS-1 operations have 50-100 flops per lattice site, i.e., they are extremely bandwidth bound. When utilizing 16-bit precision, the overall arithmetic intensity of the CG solver varies from 1.8-1.9, thus we can convert our flops number into effective sustained bandwidth by dividing by the arithmetic intensity.

To correctly report percent of peak, we cannot directly utilize the standard flops rate, since doing so would exclude the

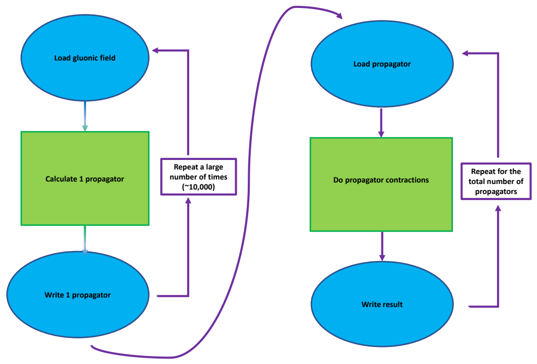
Load gluonic field
Calculate 1 propagator
Write 1 propagator
Repeat a large number of times (~10,000)
Load propagator
Do propagator contractions
Write result
Repeat for the total number of propagators

Fig. 2. The workflow of our application. I/O (blue ovals) is performed when we read a gluonic field configuration, write and read propagators, and write final results. Computation (green boxes) entails solving the Dirac equation for propagators and performing tensor contractions with those propagators.

fact that not all arithmetic operations can be issued as fused-multiply-add instructions, as well as the fact that all reductions are done in double precision. Thus when reporting percent of peak, we take into account these factors, which corresponds to approximately a $1.675\times$ scaling on the raw solver flops rate, and report the peak as a percentage of single-precision peak flops rate.

For timing these GPU performance rates we utilize timers on the CPU, ensuring to synchronicity with the GPU when start and end times are recorded.

CPU / GPU concurrency

The contractions are CPU-only tasks and due to our job manager, `mpi_jm`, we concurrently run them on the same nodes as the propagators. This completely amortizes their cost. With `mpi_jm` we carve out sections of nodes to compute propagators and do the same for contractions of previous propagators that have already been written to disk. For reading and writing we have interfaced with the parallel hdf5 library [19]. I/O takes about 0.5 % of our total application time, even after accounting for this interweaving of CPU/GPU jobs, so we do not include it in our total application budget.

Systems Tested

We have utilized the newly-installed CORAL systems, Sierra and Summit, at Oak Ridge and Livermore National Laboratories, respectively, in this work. The specifications of these systems are summarized in Table II, where we also include the prior Titan system, and the pre-CORAL development system at LLNL, Ray, which can be considered a stepping stone between Titan and Sierra/Summit since it utilizes the intermediate Pascal GPU architecture. We also show on this table the various compiler and library versions used on each machine.

On all machines we used the same physics application software. We summarize the various packages and libraries used in table III, together with specific version used, and the repositories for these packages.

Attribute	Titan	Ray	Sierra	Summit
nodes	18,688	54	$\sim$4200	$\sim$4600
GPUs / node	1	4	4	6
CPU	AMD Opteron	IBM POWER8	IBM POWER9	IBM POWER9
GPU	NVIDIA K20X	NVIDIA P100	NVIDIA V100	NVIDIA V100
FP32 TFLOPS / node	4	44	60	90
GPU bw / node GB/s	250	2880	3600	5400
CPU-GPU bw GB/s	6	20	75	50
Interconnect	Cray Gemini ($\sim$ 8 GB/s)	Mellanox IB 2xEDR	Mellanox IB 2xEDR	Mellanox IB 2xEDR
GCC	4.9.3	4.9.3	4.9.3	4.8.5
MPI	Cray MPICH 7.6.3	Spectrum 2017.04.03	MVAPICH2 2.3	Spectrum 2018.01.10
CUDA toolkit	7.5.18	9.0.176	9.2.148	9.1.85

TABLE II
COMPARISON OF THE SYSTEMS USED IN THIS STUDY

Name	commit id	repository
Lalibe	N/A	https://github.com/callat-qcd/lalibe
Chroma	72a47bd	https://github.com/JeffersonLab/chroma
QUDA	6d7f74b	https://github.com/lattice/quda
QDP++	5b711236	https://github.com/azrael417/qdpxx.git
QMP	d29f3f8	https://github.com/callat-qcd/qmp
mpi_jm	a4722f5	https://github.com/kenmcelvain/mpi_jm

TABLE III
APPLICATION SOFTWARE USED IN THIS STUDY. QDP++ WAS FORKED FROM HTTPS://GITHUB.COM/USQCD-SOFTWARE/QDPXX AND QMP WAS FORKED FROM HTTPS://GITHUB.COM/USQCD-SOFTWARE/QMP; OUR CHANGES WILL BE MERGED SOON.

VII. PERFORMANCE RESULTS

In a typical workflow, we first perform strong-scaling tests over a single propagator calculation to determine the optimal number of nodes to carve out using `mpi_jm`. We do so in figure 3, where we show the strong scaling for the $48^3 \times 64$ volume, comparing the performance over three different generations of GPU architecture. We observe that the expected behavior of increased performance with successive GPU generation is obtained, but what is more interesting is that we see the maximum percent of peak performance achieved increases with successive GPU architectures. If we convert the aggregate sustained performance in TFLOPS to bandwidth per GPU at the point of peak efficiency, e.g., lowest GPU count, we see values of 139 GB/s, 516 GB/s, and 975 GB/s for Titan, Ray and Sierra, respectively. This we attribute to the improved cache structure of successive GPUs which has seen a steady increase to both the L1 and L2 cache available per thread: this has the effect of amplifying the effective bandwidth.

In figure 4 as a next-generation proof-of-concept problem, we show strong scaling on Summit for the much larger $96^3 \times 144$ volume. As expected, a much larger problem size allows us to strong scale to a significant fraction of the machine, and the sustained solver performance approaches 1.5 PFLOPS. While this is may seem significant, we note that there is a large drop in solver efficient past $\sim$ 2000 GPUs, with dramatically reduced solver efficiency demonstrating that we cannot rely on simple data-parallel strong scaling alone in order to saturate large machines.

Instead, we utilize `mpi_jm` to determine dependencies and optimally distribute simultaneous propagators and contractions. This leads to excellent strong scaling in the number of groups that `mpi_jm` manages and allows us to sustain the highest performance from figure 3. Hardware cross interactions are negligible and from figure 5 we see that weak scaling is nearly perfect.

In figure 5 we compare weak scaling by increasing the number individual propagator solves with the number of GPUs on Sierra. We also compare this to deployment of solves with a single call to `mpi_jm`. This suffers from a slight performance hit because we used MVAPICH2 to obtain the required dynamic process management features, but have not yet fully tuned its settings for Sierra.

Figure 6 shows weak scaling on Summit with `METAQ`. Once again, our job management achieves perfect weak scaling. We would like to note, that with mpi_jm, we are able to place different jobs on different resources on a node. This has allowed us, for example, to simultaneously run independent GPU-intensive and CPU-only jobs on the same nodes. We have demonstrated this at scale on Sierra. This can be particularly advantageous for Summit and problems which do not have powers of three that nicely map onto the 6 GPUs per node. As a simple example, a set of three jobs that require 16 GPUs each can nicely be placed on 8 Summit nodes (48 GPUs). The first and second jobs can occupy GPUs 1,2,4,5 on nodes 1-4 and 5-8, while the third job can be placed on GPUs 3,6 on all 8 nodes. We have demonstrated this job placement on Summit with our workload. While the jobs that occupy 2 GPUs per node suffer a performance degredation, this can be largely mitigated by the backfilling capability of mpi_jm, such that all GPUs (and CPUs) on the node will remain occupied with new jobs as the faster ones complete and free their resources.

To compute sustained performance of our application we account for the performance of all tasks, propagator generation, contractions, and I/O. Propagators take 96.5 % of the computation, contractions take 3 %, and I/O 0.5 %. I/O is completely negligible and while our contractions account for only a small fraction, by interleaving them on the CPUs of nodes that have GPUs running propagators, their cost is brought to zero. This leaves only propagator solves, resulting in a sustained performance of 20% on the minimal number of nodes. However, when we scaled to large fractions of the machine, we relied on our job manager which, as mentioned, needed MVAPICH2. When we run a small job with MVAPICH2 we get a sustained performance equivalent to that of SpectrumMPI. When we learn how to fully utilize MVAPICH2, we anticipate bringing the sustained performance at scale from 15% to 20%, which is the right edge of figure 7.

The combination of the improvements to `QUDA` (the GPU lattice QCD library) and the development of `mpi_jm`, have allowed us to scale our workload of 4-node jobs to 3388 Sierra nodes under a single job submitted to the scheduler, with a startup time of about 5 minutes for the full set of nodes. With small improvements to `mpi_jm`, we will be able to launch a workload to the full scale of Sierra or Summit without the loss of any good nodes. At present, we have achieved

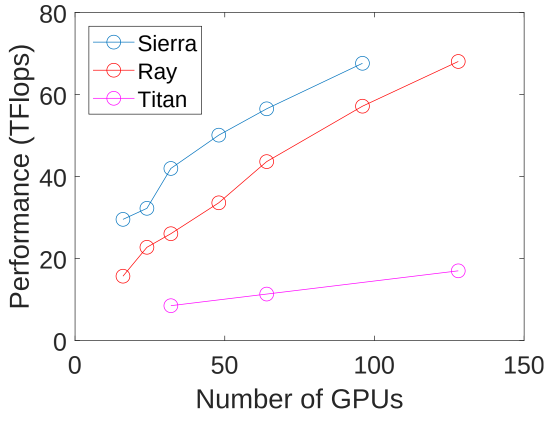

(a)

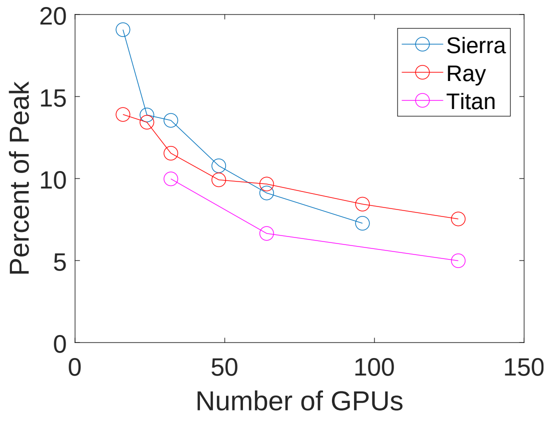

(b)

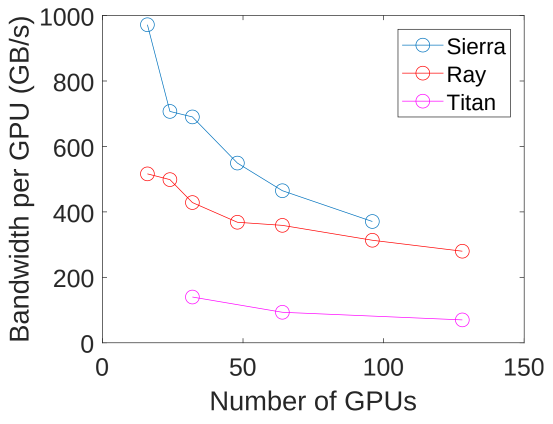

(c)

Fig. 3. Performance of QUDA's CG algorithm on Titan, Ray, and Sierra are shown above. We report performance in both TeraFlops in figure (a) and percent of peak in figure (b). All three machines are solving for a propagator on a $48^3 \times 64$ lattice. In figure (c) we give bandwidth performance, which we obtain by converting raw performance per GPU to GB/s by using an arithmetic intensity of 1.9.

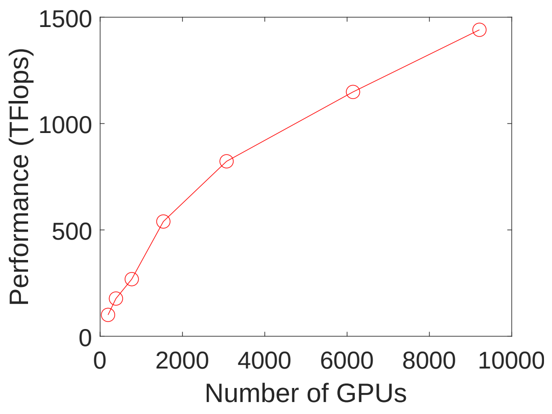

Fig. 4. Strong scaling performance of our propagator routine on Summit with a single $96^3 \times 144$ lattice.

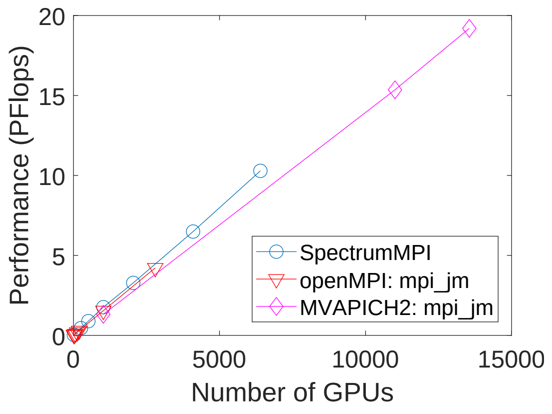

Fig. 5. The sustained performance in PFlops as the number of propagator calculations is increased. These calculations are done in groups of 4 nodes (16 GPUs) on Sierra, with a $48^3 \times 64$ lattice. The SpectrumMPI jobs were submitted as individual jobs to the scheduler, with 400 jobs submitted for the most performant run. The openMPI: mpi_jm jobs were run (in April) in up to 7 blocks of 100 nodes, where each block was a separate mpi_jm job managing the sub-tasks. The MVAPICH2: mpi_jm jobs were submitted as a single job to the scheduler with all nodes managed by a single mpi_jm task.

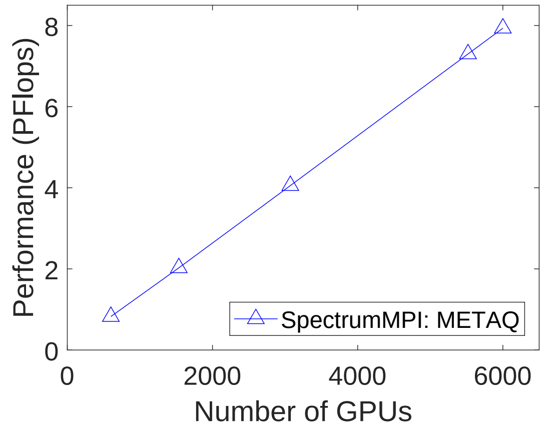

Fig. 6. The sustained performance in PFlops as the number of propagator calculations is increased. These calculations are done in groups of 4 nodes (24 GPUs) on Summit, with a $64^3 \times 96$ lattice. The jobs were managed with a single instance of METAQ that used `jsrun` to start each individual propagator task within a given allocation.

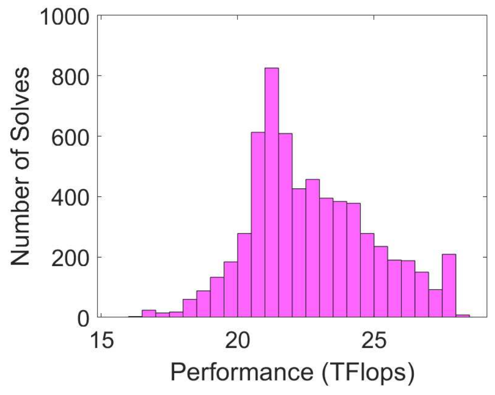

Fig. 7. Histogram of the solver performance when running on Sierra. This result is from our largest run with 13500 GPUs, using `mpi_jm` with MVAPICH2.

a peak sustained performance on Sierra of nearly 20 PFlops, which amounts to 15% of peak performance. This is the top performance in a single job-submission that has been achieved for lattice QCD to date. Stated differently, the machine-to-machine speed up of Sierra and Summit over Titan, for our research program, is a factor of approximately 12 and 15 respectively. These CORAL machines are truly disruptive and we look forward to using them as extensively as possible.

ACKNOWLEDGEMENTS

We are indebted to the Livermore Computing Center for access to Sierra and help getting set up there. In particular, our contacts John Gyllenhal, Adam Bertsch and Py Watson were very helpful and responsive. Our other Livermore colleagues who also applied for an award were very cooperative and collaborative, keeping us appraised of the state of the machine, difficulties they encountered, and workarounds. In particular, Jim Glosli, Tomas Oppelstrup, and especially Tom Scogland were very generous with their time and concern. At the Oak Ridge Leadership Computing Facility, Jack Wells provided excellent help, advice, and encouragement.

An award of computer time was provided by the Innovative and Novel Computational Impact on Theory and Experiment (INCITE) program to CalLat (2016) as well as the Lawrence Livermore National Laboratory (LLNL) Multiprogrammatic and Institutional Computing program through a Tier 1 Grand Challenge award. This research used the NVIDIA GPU-accelerated Titan, Summit-Dev, and Summit supercomputers at the Oak Ridge Leadership Computing Facility at the Oak Ridge National Laboratory, which is supported by the Office of Science of the U.S. Department of Energy under Contract No. DE-AC05-00OR22725, and the NVIDIA GPU-accelerated Surface, Ray, and Sierra supercomputers LLNL. This work was performed under the auspices of the U.S. Department of Energy by LLNL under Contract No. DE-AC52-07NA27344 and under contract DE-AC02-05CH11231, which the Regents of the University of California manage and operate Lawrence Berkeley National Laboratory and the National Energy Research Scientific Computing Center

References

[1] C. Patrignani *et al.*, "Review of Particle Physics," *Chin. Phys.*, vol. C40, no. 10, p. 100001, 2016.

[2] A. Czarnecki, W. J. Marciano, and A. Sirlin, "The Neutron Lifetime and Axial Coupling Connection," 2018.

[3] B. Fornal and B. Grinstein, "Dark Matter Interpretation of the Neutron Decay Anomaly," 2018.

[4] Z. Tang *et al.*, "Search for the Neutron Decay n$\rightarrow$ X+γ where X is a dark matter particle," 2018.

[5] A. P. Serebrov, R. M. Samoilov, I. A. Mitropolsky, and A. M. Gagarsky, "Neutron lifetime, dark matter and search for sterile neutrino," 2018.

[6] Science Talk 1: Cold Nuclear Physics, USQCD Annual Progress Review to the US DOE, http://www.usqcd.org/reviews/June2016Review/agenda.html; Nuclear Physics Exascale Requirements Review, https://science.energy.gov/~/media/ascr/pdf/programdocuments/docs/2017/DOE-ExascaleReport-NP-Final.pdf.

[7] C. Bouchard, C. C. Chang, T. Kurth, K. Orginos, and A. Walker-Loud, "On the Feynman-Hellmann Theorem in Quantum Field Theory and the Calculation of Matrix Elements," *Phys. Rev.*, vol. D96, no. 1, p. 014504, 2017.

[8] E. Berkowitz, C. Bouchard, D. B. Brantley, C. Chang, M. Clark, N. Garron, B. Joó, T. Kurth, C. Monahan, H. Monge-Camacho, A. Nicholson, K. Orginos, E. Rinaldi, P. Vranas, and A. Walker-Loud, "An accurate calculation of the nucleon axial charge with lattice QCD," 2017.

[9] C. Chang, A. Nicholson, E. Rinaldi, E. Berkowitz, N. Garron, D. B. Brantley, H. Monge-Camacho, C. Monahan, C. Bouchard, M. Clark, B. Joó, T. Kurth, K. Orginos, P. Vranas, and A. Walker-Loud, "Nucleon axial coupling from Lattice QCD," in *35th International Symposium on Lattice Field Theory (Lattice 2017) Granada, Spain, June 18-24, 2017*, 2017. [Online]. Available: http://inspirehep.net/record/1631340/files/arXiv:1710.06523.pdf

[10] C. C. Chang *et al.*, "A per-cent-level determination of the nucleon axial coupling from quantum chromodynamics," *Nature*, vol. 558, no. 7708, pp. 91–94, 2018.

[11] R. G. Edwards and B. Joó, "The Chroma software system for lattice QCD," *Nucl. Phys. Proc. Suppl.*, vol. 140, p. 832, 2005.

[12] http://usqcd-software.github.io, 2018, commit `a4722f5`.

[13] M. A. Clark, R. Babich, K. Barros, R. C. Brower, and C. Rebbi, "Solving Lattice QCD systems of equations using mixed precision solvers on GPUs," *Comput. Phys. Commun.*, vol. 181, pp. 1517–1528, 2010.

[14] E. Berkowitz, "`METAQ`: Bundle Supercomputing Tasks," 2017. [Online]. Available: https://github.com/evanberkowitz/metaq

[15] E. Berkowitz, G. R. Jansen, K. McElvain, and A. Walker-Loud, "Job Management and Task Bundling," *EPJ Web Conf.*, vol. 175, p. 09007, 2018.

[16] "`MPICH`," https://www.mpich.org, 2018.

[17] "`MVAPICH2`," lhttp://mvapich.cse.ohio-state.edu, 2018.

[18] "`QMP` (QCD Message Passing)," http://usqcd-software.github.io/qmp, 2004.

[19] T. Kurth, A. Pochinsky, A. Sarje, S. Syritsyn, and A. Walker-Loud, "High-Performance I/O: HDF5 for Lattice QCD," *PoS*, vol. LATTICE2014, p. 045, 2015.